HHS Public Access

Author manuscript

Ecotoxicol Environ Saf. Author manuscript; available in PMC 2023 March 01.

Published in final edited form as:

Ecotoxicol Environ Saf. 2022 March 01; 232: 113239. doi:10.1016/j.ecoenv.2022.113239.

Polystyrene bead ingestion promotes adiposity and cardiometabolic disease in mice

Jingjing Zhao[1], **Daniel Gomes**[1,2], **Lexiao Jin**[1], **Steven P. Mathis**[3], **Xiaohong Li**[4,5], **Eric C. Rouchka**[4,6], **Haribabu Bodduluri**[3], **Daniel J. Conklin**[1], **Timothy E. O'Toole**[1,*]

[1]Christina Lee Brown Envirome Institute, Department of Medicine, University of Louisville, Louisville, KY, USA.

[2]Department of Pharmacology and Toxicology, University of Louisville, Louisville, KY, USA.

[3]Department of Microbiology and Immunology, James Graham Brown Cancer Center and Center for Microbiomics, Inflammation and Pathogenicity, University of Louisville, Louisville, KY, USA.

[4]Kentucky Biomedical Research Infrastructure Network Bioinformatics Core, University of Louisville, Louisville, KY, USA

[5]Department of Anatomical Sciences and Neurobiology, University of Louisville, Louisville, KY, USA

[6]Department of Computer Science and Engineering, University of Louisville, Louisville, KY, USA.

Abstract

Vast amounts of plastic materials are produced in the modern world and despite recycling efforts, large amounts are disposed in water systems and landfills. Under these storage conditions, physical weathering and photochemical processes break down these materials into smaller particles of the micro- and nano-scale. In addition, ecosystems can be contaminated with plastic particles which are manufactured in these size ranges for commercial purposes. Independent of source, microplastics are abundant in the environment and have found their way into water supplies and the food cycle where human exposure is inevitable. Nevertheless, the health consequences of microplastic ingestion, inhalation, or absorption are largely unknown. In this study we sought to determine if ingestion of microplastics promoted pre-clinical cardiovascular

*Corresponding author University of Louisville, 302 E. Muhammad Ali Blvd., Louisville, KY USA 40202, tim.otoole@louisville.edu, 502-852-5886.

AUTHORS' CONTRIBUTIONS

Study design: JZ/HB/DJC/TEO. Data collection: JZ/DG/LJ/SPM/TEO: Data analysis and interpretation: JZ/LJ/XL/ECR/DJC/TEO. Manuscript draft: JZ/SPM/XL/HB/DJC/TEO. Supervision and coordination of the study: TEO. Critical revision and final decision to submit: all authors. The author(s) read and approved the final manuscript

DECLARATIONS

The animal studies were approved by the University of Louisville IACUC (#19654). The authors declare they have no competing interests.

Declaration of interests

The authors declare that they have no known competing financial interests or personal relationships that could have appeared to influence the work reported in this paper.

disease (CVD). To do this, we supplied mice with normal drinking water or that supplemented with polystyrene beads of two different sizes (0.5μm and 5μm) and two different doses (0.1μg/ml and 1μg/ml) each for 12 weeks and measured several indices of metabolism and glucose homeostasis. As early as 3 weeks of consumption, we observed an accelerated weight gain with a corresponding increase in body fat for some exposure groups versus the control mice. Some exposure groups demonstrated increased levels of fasting plasma glucose. Those mice consuming the smaller sized beads (0.5μm) at the higher dose (1μg/ml), had increased levels of fasting plasma insulin and higher homeostatic model assessment of insulin resistance (HOMA-IR) scores as well. This was accompanied by changes in the gut microbiome consistent with an obese phenotype. Using samples of perivascular adipose tissue collected from the same group, we observed changes in gene expression consistent with increased adipogenesis. These results suggest that ingestion of polystyrene beads promotes a cardiometabolic disease phenotype and thus may be an unrecognized risk factor for CVD.

Keywords

microplastics; polystyrene; cardiometabolic disease; obesity; gut microbiome

1. INTRODUCTION

Modern society produces enormous amounts of plastics, which find widespread use in consumer products, packaging, and clothing. Current estimates suggest that 364 million tons of plastics are produced annually and that this number will triple by 2050 (1). While some of this plastic material is recycled, vast amounts are disposed, ultimately ending up in landfills and water systems. In these conditions, there is a slow but persistent physicochemical degradation of plastics into particles of smaller sizes, the smallest of which are <100μm. These so called “secondary” microplastics (MP) are generated by fragmentation from larger polymers through wind shear, abrasion and/or weakening from photo- and thermo-oxidative processes. In addition to fragmentation from larger polymers, there is wide-spread deposition of “primary” MP, which are specifically engineered in this size range for manufacturing or commercial purposes. Additional MP and fibers of many sizes are shed from synthetic textiles during normal wear and tear and during laundry and drying, and can be generated from the abrasion of materials such as tires. Independent of source, multiple studies have shown that MP of all sizes are becoming increasingly pervasive in both aquatic and terrestrial ecosystems. Given this ubiquitous distribution, MP have found their way into water supplies and the food chain (2), where they are ultimately consumed by humans.

While it is becoming increasingly clear that humans are exposed to MP from multiple sources and by many means, the health consequences of such exposures are less clear. The potential toxicity of MP derives mostly from their physical and chemical properties. Because of their small size, inhaled or ingested MP can be absorbed by epithelial cells in the lungs or gut (3, 4), where they have been reported to trigger immune responses, promote the generation of reactive oxygen species (ROS) and increase permeability (1, 5). Smaller sized MP have also been found in circulation (6) and have been shown

to cross placental barriers (7). Due to their large surface area and hydrophobicity, MP can effectively bind microorganisms or chemicals and ingestion of these laden MP can concentrate absorbed toxins in susceptible tissues or potentiate their effects (5). An understanding of the physiological responses resulting from MP ingestion is in its infancy. Early evidence suggests some outcomes may be dependent upon MP size, dose, and the extent of bioaccumulation in a given cell or tissue type (8, 9). Some reported outcomes of MP ingestion appear to be an induction of inflammatory responses (10, 11), increased ROS production (3), altered cellular bioenergetics (12, 13), enhanced thrombogenicity (5), and alterations in microbiome composition and/or metabolism (14, 15).

Cardiovascular disease (CVD) is the leading cause of mortality worldwide, affecting both genders, all ethnicities, and all socioeconomic classes (16). CVD arises from a complex interplay of genetic and life-style factors which collectively alter the structure or impair the function of vascular and cardiac tissues. While some CVD can be attributed to aging and is thus unavoidable, existing evidence suggests that a large percentage of CVD derives from modifiable risk factors and is thus preventable (16). Indeed, improvements in diet, increased physical activity, cessation of smoking, and effective pharmaceutical interventions have limited the incidence and somewhat alleviated the severity of CVD. Yet CVD persists and its frequency is even increasing in parts of the world. Likewise, metabolic disorders such as diabetes and obesity, significant contributors to CVD, are also increasing worldwide. The persistence of these disorders suggests that environmental factors may play a prominent role in their genesis and progression.

Given that MP ingestion by humans or mice promotes inflammation, ROS production, and changes in the gut microbiome, and that these outcomes also underlie metabolic disorders, it remains plausible that MP exposure is an environmental risk factor for CVD. To test this, we studied the effects of polystyrene (PS) exposure in mice. PS, together with polyethylene and polypropylene comprise an estimated 56% of global plastic waste and a similarly large percentage of those plastics most likely to be ingested (17, 18). PS ingestion may be particularly harmful to health. It is prone to degradation by heat and acid conditions, leaching absorbed chemicals and degradation products such as benzoic acid (19). In addition, its monomer, styrene, is a known carcinogen and neurotoxin (20, 21). To study the impact of PS ingestion on CVD, we supplied mice with water containing different sizes and doses of PS beads and examined indices of metabolism and glucose homeostasis over time. Our results suggest a size and dose-dependent association between exposure and increased adiposity, hyperglycemia, and homeostatic model assessment of insulin resistance (HOMA-IR) scores. Thus, MP exposure in general, and PS exposure in particular, may be a here-to-fore unrecognized risk factor for CVD.

2. METHODS

2.1 Animals and treatment

Male C57BL/6 mice at 12 weeks old were purchased from Jackson Laboratories (Bar Harbor, ME. USA) and housed (5 per cage) in AALAC- and USDA-accredited facilities at UofL. Two bead stock solutions (Creative Diagnostics; Shirley, NY. USA) were obtained: “5μm” beads (range = 4.5 - 4.9μm) 5.0% w/v dispersed in DI water (8.28×10^8 particles/

ml); and "0.5μm" beads (range = 0.4 – 0.6μm) 5.0% w/v dispersed in DI water (1.4 $\times 10^{12}$ particles/ml). After one week of acclimation, randomly selected cages of mice (2 cages; n=10) were maintained on normal (filtered, autoclaved) water or normal containing polystyrene beads. For the latter, four treatment groups were used, consisting of two doses (0.1μg/ml and 1.0μg/ml) for each of the two bead sizes (0.5μm and 5μm). Assuming the mice drink 3.6ml of water per day (metabolic cage data), it is thus estimated they would consume 0.36μg or 3.6μg daily. The experimental outline is illustrated in Figure 1. Fresh water solutions were prepared every other day, and to limit aggregation, stock bead solutions were sonicated for 30 minutes prior to dilution. On those days when fresh water was not supplied, existing water bottles were agitated to limit potential bead settling. The mice had access to their water supplies *ad libitum* and were maintained in these conditions for 12 weeks Mice were euthanized by sodium pentobarbital (150 mg/kg body weight) injection.

2.2 Metabolic analysis

Body weights were recorded every three weeks during the treatment protocol and after 9 weeks of treatment, body mass analysis was obtained by Lunar (Chicago, Il. USA) PIXlmus Dual Energy X-ray Absorptiometer (DEXA) scanning. Fasting plasma glucose levels were obtained every three weeks using a glucometer (Accu-Chek, Aviva; Indianapolis, IN. USA) and appropriate test strips (Accu-Chek, Aviva Plus). Glucose tolerance tests (GTTs) were performed on all groups after 9wk of consumption while insulin tolerance tests (ITTs) were performed on control mice and that group demonstrating the largest change in fasting plasma glucose (i.e. consuming 0.5μm beads at a dose of 1.0 μg/ml). Both GTT and ITT were performed after 6hr of fasting. Respective areas under the curve (AUC) for GTT and areas above the curve (AAC) for ITT were calculated using the trapezoid rule (22). The metabolic phenotype (food and water intake, O_2 consumption, CO_2 production, respiratory exchange ratio, physical activity) of control mice and those mice demonstrating the largest change in fasting plasma glucose (i.e. consuming 0.5μm beads at a dose of 1.0 μg/ml) was determined by 24hr housing in a TSE PhenoMaster/LabMaster Metabolic Chamber System (Chesterfield, MO. USA).

2.3 Blood parameters

Blood was obtained from euthanized mice by cardiac puncture using 0.2M EDTA as an anticoagulant. Complete blood cell counting was done on an aliquot using a Drew Scientific Hemavet 950FS (Miami Lakes, FL. USA). Plasma was isolated from the remaining blood and aliquots were used to measure insulin by ELISA (Millipore; Burlington, MA. USA), and total plasma cholesterol, HDL, low density lipoprotein (LDL), and triglycerides using an Axcel Clinical Chemistry Analyzer (West Caldwell, NJ. USA). HOMA IR - scores were calculated as described (23).

2.4 Adipogenesis gene array and qRT-PCR

After euthanasia, perivascular adipose tissue (PVAT) was collected from 4 mice drinking normal water and 4 mice from group 5 (consuming the 0.5μm beads at a dose of 1μg/ml). Total RNA was isolated from this tissue using the miRNeasy kit (Qiagen; Germantown, MD. USA), and equal amounts from each of the groups were pooled to prepare cDNAs using the RT^2 first strand kit (Qiagen). These samples were then used to screen an adipogenesis

gene array (Qiagen) as per manufacturer's suggestions. Fold changes were calculated using the $\Delta\Delta C_T$ method (Supplementary Table 1). Changes in the expression of Irs2, Bmp7, and Wnt-1 were also confirmed by additional RT-PCR analysis using individual rather than pooled RNA samples.

2.5 Microbiome analysis

Feces was collected from mice drinking normal water and group 5 mice (consuming the 0.5μm beads at a dose of 1μg/ml) after 12 weeks of exposure. Microbial genomic DNA was extracted from frozen fecal samples using the FastDNA Spin Kit for Feces (MP Biomedicals; Irvine, CA. USA) as per manufacturer's instructions and quantified using High Sensitivity Qubit reagent (Thermo Fisher; Waltham, MA. USA). To prepare libraries, 10ng of input DNA was used to amplify the full length 16s gene using the LongAMP Hot Start Master mix (New England Biolabs; Ipswich, MA. USA) and barcoded primers (Oxford Nanopore Technologies; Cambridge, MA. USA). Amplified products were cleaned up using AMPure XP beads and quantified as above. Sequencing was performed on equal amounts of the samples at the University of Louisville Functional Microbiomics Core using MinION instrumentation (Oxford Nanopore Technologies). Raw reads in fast5 format were de-multiplexed using deepbinner. Base-calling and conversion into fastq format was performed in Guppy (version 3.2.10; Oxford Nanopore Technologies).

Sequence data from each of the samples consisted of 14 to 33 single-end fastq files that were concatenated into a single fastq file using a unix *cat* command. Porechop (24) and Nanofilt (25) tools were used for adapter trimming and quality filtering with a score ≥ 9. Quality control of the 20 raw sequences and trimmed data was performed using FastQC (version 0.10.1) and the trimmed files had a median quality score ≥ 16 with 97.5% accuracy. The total reads of each sample before and after trimming are listed in the Supplemental Table 2. The trimmed files were locally aligned against the Silva reference (SILVA_132_QIIME_release) using BLASTn (ncbi-blast-2.10.1) comand line written in a perl script with an e-value cut-off of 1e-90 (26). The outputs from BLASTn were merged into an operating taxonomy unit (OTUs) matrix that was further filtered by zero counts and minmum frequency of 2 across the 20 samples. The filtered OTU matrix was used to generate representative sequences with 99% similarity usig a perl script. The OTU matrix and representative sequence files were imported into QIIME2 and converted as a feature table (table.qza) and representative sequences sets (rep-set.qza) for the downstream analysis. The feature table was rarefied at subsampling a minimum read depth of 3,918,982 for core diversity analysis, which is used for taxonomy analysis between two groups. The rep-set.qza was used to generate a phylogenetic tree and combined with the feature table for the alpha and beta diversity, richness and UniFrac analysis. The *Emperor* tool was used to explore the principal coordinate analysis (PCOA) plot in the context of sample metadata which is the distance between samples (beta diversity) using weighted and/or unweighted UniFrac. Linear discriminant analysis (LDA) effect size (LEfSe) method was used to find the most differentially abundant enriched microbial taxa between the groups in different levels. The analysis was performed on the Galaxy platform using taxonomy results from QIIME 2 and the results were illustrated by histograms with LDA score ≥2 and significance α <0.05 as determined by nonparametric Kruskal-Wallis test. The statistical difference of alpha

diversity of gut microbiota was assessed using a nonparametric Kruskal-Wallis test within Qiime 2. The statistical significance in beta diversisty of gut microbiota between two groups was based on permutation ANOVA (PERMANOVA) test with the aid of Qiime 2.

2.6 Vascular Function

Thoracic aortas were assayed for vascular reactivity as described with modification (27). Briefly, one 3-4-mm aortic ring per mouse (cleaned of PVAT) was hung on stainless steel hook in water-jacketed organ baths (37°C) in physiological salt solution (PSS:119 mM NaCl, 4.7 mM KCl, 1.2 mM $MgSO_4$η$7H_2O$, 1.2 mM KH_2PO_4, 25 mM $NaHCO_3$, 1.6 mM $CaCl_2$, 11.1 mM glucose, pH 7.4) (28) and bubbled with 95% O_2 and 5% CO_2. Rings (≈1 g loading tension) were contracted with 100 mM potassium solution (twice, separately), washed with 3 bath changes of PSS between stimulations, and re-equilibrated to ≈1 g resting tension over ≈1.5 h. For phenylephrine (PE) contraction, PE was added in cumulative concentrations (0.1 nM-10 μM). For endothelium-dependent relaxation, PE-pre-contracted (10 μM) aortas were relaxed with cumulative concentrations of acetylcholine (ACh; 0.1 nM-10 μM). For endothelium-independent relaxation, PE-pre-contracted aortas were relaxed with cumulative concentrations of sodium nitroprusside (SNP; 0.1 nM-100 μM). To assess specific contribution of nitric oxide synthase (NOS) to PE function, L-NAME (100 μM) was added to bath after PE-induced tension had plateaued. The resulting increased tension was ‘PE+L-NAME tension’ and a ‘PE Contraction Ratio’ was calculated as follows: PE+L-NAME Tension / PE Tension. Relaxation efficacy was calculated as a percentage reduction of agonist-induced tension. Agonist-induced contraction was normalized to aortic ring length (mN/mm). The effective concentration producing 50% response (EC_{50}) was assessed for each agonist by normalizing cumulative concentration responses to 100% response, plotting the % response vs. the log $[molar]_{agonist}$, with subsequent interpolation of the EC_{50}. The pD_2 was calculated as the $-\log(EC_{50})$.

3. RESULTS

3.1 Polystyrene consumption induces adiposity

To determine if consumption of PS beads impacts body weight, animals in the four treatment groups and the control group were weighed every 3 weeks during the exposure time course. As early as 3 weeks of consumption, we observed that three treatment groups (groups 3-5) had an increase in body weight that was significantly greater than that in control mice (Figure 2A, B). While weight changes from baseline varied at subsequent time points, after both 9 and 12 weeks of consumption, mice from group 3 (1μg/ml; 5μm beads) and group 5 (1μg/ml; 0.5μm beads) had significant increases compared with control mice (Figures 2A, B). To determine body composition, we performed a dual energy X-ray absorptiometery (DEXA) scan analysis after 9wk of PS consumption (Figures 2 C, D). At this time point, mice from three treatment groups (groups 3-5) demonstrated an increase in percentage body fat versus control mice.

3.2 Polystyrene consumption and metabolic phenotype

Obesity is often associated with a disruption of glucose homeostasis. To determine if consumption of PS beads impacted this outcome, we initially measured fasting plasma

glucose levels every 3 weeks during the exposure time course. After 3wk of consumption, three treatment groups (groups 2,4,5) demonstrated increased glucose levels compared to control (Figures 3A, B). While absolute glucose levels varied and actually decreased during the subsequent weeks, after 12wk of consumption, those mice in group 5 (1μg/ml: 0.5μm beads) had significantly higher levels than control mice (Figure 3B). To further assess glucose handling, we performed both glucose tolerance tests (GTT) and insulin tolerance tests (ITT). A GTT performed using all groups demonstrated no differences between these groups (Supplemental Figure 1A). Given that mice from group 5 (1μg/ml; 0.5μm beads) had the highest glucose levels after 12wk of consumption, they were used in an ITT. However, in this analysis, we also observed no differences between this group and control mice (Supplemental Figure 1B).

We next measured fasting plasma insulin levels in all mice at termination. While most groups demonstrated no difference from control, those mice in group 5 (1μg/ml; 0.5μm beads) did have significantly higher levels of insulin (Figure 3C). Consistently, mice from this group also had higher HOMA-IR scores than control mice (Figure 3D). When we measured plasma lipids, we observed a minor but statistically significant increase in high density lipoprotein (HDL) in the same exposure group (Supplemental Table 3), while were no other differences between the control and exposure groups in other lipid measures. Finally, we assessed the metabolic activity of control mice and those mice in group 5 (1μg/ml; 0.5μm beads)). This was done by housing the mice in a metabolic chamber, which records several parameters of nutrient uptake, respiration, and physical activity. No differences were observed between the two groups when we analyzed these parameters in the dark phase (6PM to 6AM), or most active hours of the murine circadian cycle (Supplemental Table 4).

3.3 Polystyrene consumption and hematopoiesis

The inhalation or tracheal installation of air pollution particulate matter impairs the abundance or proliferation of bone marrow stem cells in mice (29, 30), implying an imbalance of circulating blood cells populations over time. To determine if PS bead exposure might induce a similar outcome, we determined complete blood cell counts in all groups at termination. While there were no changes between the control and PS exposure groups for most cell types, we did observe that levels of eosinophils and basophils were increased, but this change was apparent only in those mice consuming the 5μm beads (groups 2, 3), but not the 0.5μm beads (groups 4, 5) (Table 1). We also observed an increase in monocytes in group 3 mice (1μg/ml; 5μm beads).

3.4 Polystyrene consumption and vascular function

To assess potential vascular effects of PS consumption, we assessed vascular contractility and relaxation in thoracic aorta *ex vivo*. We quantified measures of both aortic efficacy and sensitivity to contractile and relaxant agonists. Noticeably, in PS-exposed mice (groups 4, 5: 0.1μg/ml and 1.0μg/ml; 0.5μm beads), aortic contractile efficacy appeared suppressed while the sensitivity to PE appeared shifted slightly to the left (enhanced) (Supplemental Figure 2A, B; Supplementary Table 5). Because no obvious dose dependence was observed, we also tested whether combining the data from both the doses (0.1μg/ml and 1.0μg/ml)

was different from control. In fact, PS consumption significantly enhanced aortic sensitivity to phenylephrine (PE) by 1.75-fold compared with control (EC_{50} control: 61.6±10.7 nM; EC_{50} $PS_{combined}$: 35.2±5.5 nM; n=5, 10, respectively; $p<0.05$; Supplementary Table 5). Because PE-induced contractions are modulated by relaxing factors released from the endothelium, we measured relaxations to endothelial-dependent and -independent agonists. As in a previous study of short-term air pollution exposure (31), we did not observe frank endothelial dysfunction in aortas after PS consumption (Supplemental Figure 2C). However, there was a subtle lessening of the sensitivity of ACh-induced relaxation (Supplemental Figure 2D; Supplementary Table 5), although it did not reach statistical significance and did not display dose dependence. In concordance, the PE Contraction Ratio (i.e., $Tension_{PE+L\text{-}NAME}/Tension_{PE}$), which quantifies how much contractile modulation is due to nitric oxide synthase (NOS), also was not different between groups (Supplementary Table 5). No changes in efficacy or sensitivity of aortas in response to the NO donor, SNP, were observed (Supplemental Figure 2 E, F; Supplementary Table 4). Collectively, these data indicate that PS consumption induced a mild sensitization of aortic smooth muscle to alpha adrenergic receptor agonists (i.e., catecholamines) in the absence of increased contractility or overt endothelial dysfunction.

3.5 Polystyrene consumption and perivascular adipose tissue (PVAT) gene expression

Adipose expansion is associated with CVD and prior evidence has specifically linked PVAT dysfunction to atherogenesis (32). To determine if PS consumption promoted PVAT dysfunction, we collected this tissue at termination from control mice and group 5 mice (1μg/ml: 0.5μm beads). RNA was isolated from these tissues and pooled samples were then used to screen an adipogenesis gene expression array. From this analysis, we observed that 5 genes were up-regulated by at least 1.5-fold (fold change >1.5) versus control mice, while 14 genes were down-regulated by at least 1.5-fold (fold change <0.66) (Table 2). Calculated fold changes for all genes in the array are listed in Supplemental Table 1. To confirm some of these results, we used individual RNA samples, and performed rtPCR for Irs2, Bmp7, and Wnt-1, which were among the most up-regulated or down-regulated. Analysis of these results (Table 2) identified similar trends with regards to expression levels. As adipose tissue expansion is also associated with inflammation, we finally analyzed the expression of some pro-inflammatory genes, not included in the array analysis. Consistent with a pro-inflammatory phenotype, both interleukin-6 (*IL-6*) and monocyte chemoattractant protein-1 (*Mcp-1*), were up-regulated in PVAT samples obtained from the PS-exposed mice (Table 2).

3.6 Polystyrene consumption and microbiome

The identity and relative abundance of distinct bacterial populations in the gut is associated with increased obesity (33-35). To determine if PS consumption altered gut microbiome composition, we collected feces from control mice and group 5 mice (1μg/ml; 0.5μm beads), which demonstrated the greatest increase in weight and fasting plasma glucose after 12wk of consumption. DNA was then isolated and used in 16s rRNA sequencing. In this analysis we observed a decrease in β-diversity in those mice drinking the water containing PS beads (Figure 4A, B) as well as discrete changes in bacterial phyla (Figure 4C) and genus (Supplemental Figure 3). The two most abundant phyla are the Firmicutes and Bacteriodetes

and we observed a relative increase of Firmicutes in mice consuming the PS-containing water (Figure 5). Additional PS-associated changes were observed in the lesser-abundant phyla (Figure 5).

4. DISCUSSION

The major finding of this study is that ingestion of PS beads by mice promotes an increase in obesity in a dose and size dependent manner. Furthermore, this phenotype was accompanied, at least in those mice consuming the 0.5μm beads at a dose of 1μg/ml, by hyperinsulinemia, elevated HOMA-IR scores, and changes in the gut microbiome that are associated with increased adiposity. We also detected elevated plasma glucose levels and changes in peripheral blood cells in some exposure groups as well as gene expression changes in PVAT which are consistent with the dysfunction of this tissue and its role in atherogenesis. These results suggest that the inevitable consumption of environmentally ubiquitous microplastic particles by humans may be a here-to-fore unrecognized risk factor for the development of CVD.

An increase in the body weights of exposed mice versus controls was observed as early as 3 weeks after initiation of treatment. Increases at this time point were more prominent in those mice consuming the smaller sized beads (0.5μm). While there was some fluctuation in body weight changes throughout the remainder of the exposure duration, mice receiving the higher dose (1μg/ml) of either bead size displayed significant weight changes after both 9 and 12 weeks of exposure. This increase in body weight was apparently due to an increase in percent fat as evidenced in our DEXA scan analysis performed after 9 weeks of exposure. Adiposity is often associated with impaired glucose handling and, consistent with the weight gain at 3 weeks of exposure, we observed that several groups had increased levels of plasma glucose at this time point. At termination of treatment, mice consuming the higher dose (1.0μg/ml) of the smaller size (0.5μm) beads demonstrated significantly higher glucose levels versus the control mice. We observed increases in fasting plasma glucose despite no observed changes in a glucose tolerance test in all groups or in an insulin tolerance test using those mice demonstrating the largest difference in glucose levels at 12 weeks. One group (1.0μg/ml; 0.5μm beads), demonstrated an increase in fasting plasma insulin as well as increases in HOMA-IR scores. Finally, in this same group, we observed statistically significant increases in HDL. Our observed increase in weight differs from an earlier study which identified no weight changes in animals ingesting 5μm PS beads at several doses (3). The basis of this difference is uncertain but may result from differences in routes of exposure or exposure duration. Likewise, while we observed no changes in total cholesterol and triglycerides after 12 weeks of exposure, other reports identified decreases in these parameters in exposed animals (3, 14, 15). These differences may likewise be a consequence of variations in experimental protocols.

One mechanism potentially contributing to the increased adiposity we observed, is PS-induced changes in the gut microbiome. In our analysis of bacterial phylum, we observed an increase in the relative abundance of Firmicutes over Bacteriodetes in those animals consuming the PS beads. Consistent with our findings, prior studies have also suggested that an increased Firmicutes/Bacteriodetes ratio is associated with obesity in mice and humans

(34, 35). In addition, obesity is associated with reduced microbiota diversity and richness (34, 35), and we likewise observed a decreased beta diversity in mice consuming PS beads. Prior studies have similarly shown that the ingestion of microplastics alters the composition of the gut microbiome or gut barrier function (14, 15). The reasons whereby gut microbes promote obesity are complex but may involve the increased production of short chain fatty acids, decreased fatty acid oxidation, altered bile acid circulation and altered immune responses (34, 35). A detailed analysis of the role of microbiota in PS-induced obesity and the mechanisms thereof require further study.

The increased obesity and hyperglycemia we observed are some of the defining characteristics of the metabolic syndrome, a series of related disorders which elevates the risk of developing CVD (36). In addition to increased abundance, adipose tissue dysfunction, and PVAT dysfunction in particular, has also been linked to CVD and atherogenesis (32). Thus, to determine if PS consumption might alter the properties or function of PVAT, we screened a gene array for adipogenesis-related genes. Among the most up-regulated and down-regulated genes identified in the array and confirmed by rtPCR were some involved in Wnt signaling. This signaling pathway is essential for embryonic development and cell differentiation in general, and adipocyte differentiation in particular (37, 38). In canonical Wnt signaling, when a Wnt family member binds to its cell surface receptor, a complex of Frizzled (FZD) family proteins with low density lipoprotein-receptor-related protein (LRP), an intracellular, receptor-associated protein, β-catenin, is protected from ubiquitination and degradation. In this scenario, β-catenin can be translocated to the nucleus where it promotes the expression of Wnt-target genes. This active signaling mechanism promotes the osteogenic and myogenic differentiation of mesenchymal stem cells at the expense of adipocyte differentiation. However, in the absence of Wnt-receptor ligation or effective Wnt signaling, β-catenin is targeted for ubiquitination and degradation, negating its nuclear translocation and thereby, promoting adipocyte differentiation. Consistent with the enhanced adiposity we observed in PS-fed animals, Wnt-1 expression was significantly decreased (0.407-fold) in collected PVAT samples. Furthermore, Dickkopf homolog 1 (Dkk1), which antagonizes Wnt binding to the FZD/LRP complex (38), was identified as the most up-regulated gene (4.23-fold) in the same tissue. In addition to these changes directly impairing Wnt signaling, we identified other transcription factors and signaling molecules whose down-regulation promotes adipocyte differentiation or increases in obesity. Among these include Gata3 (fold change: 0.051) (39), Nr0b2 (fold change: 0.425) (40), Cdkn1b (fold change: 0.491) (41), and Creb1(fold change: 0.554) (42). In addition, from the array we detected altered expression of certain genes regulating the “browning” of white adipose tissue (WAT). Browning is an adaptation of adipose converting that with an energy storage, “white” phenotype to a mitochondrial-rich, and metabolically active “brown” phenotype (brown adipose tissue: BAT), which is important for thermogenesis. We observed that Bmp7, which strongly promotes browning (43), was down-regulated (0.172 fold), as was Nrf1 (fold change: 0.511), which promotes BAT function and whose deficiency promotes “whitening” (44). Finally, we also observed an increase in the expression of *IL-6* and *Mcp-1* in the collected PVAT samples. The up-regulation of these pro-inflammatory mediators is consistent with obesity-associated adipose tissue dysfunction and the role of dysfunctional PVAT in the pathogenesis of atherosclerosis

(32). Thus, ingestion of PS beads induces genes expression changes in PVAT consistent with “whitening” or the accumulation of metabolically inactive, pro-inflammatory WAT. Consistent with this pro-atherogenic potential, we also observed changes in endothelial reactivity (Supplemental Figure 2).

Another intriguing finding of this initial study was the PS size-dependent increase in circulating eosinophils and basophils. This outcome was apparent in those mice ingesting beads of the 5μm size of either dose, but not in those mice ingesting beads of the 0.5μm size. The basis of this differential response is uncertain but may be due to differences in the distribution and tissue accumulation of these different sized particles. Results from earlier studies on the bioaccumulation of PS beads remain controversial. While with some provided evidence that ingested beads could accumulate in several tissues dependent upon size (3), other studies suggest a more limited distribution (4) or little to none at all (9). How the beads used in the current study were sequestered and localized after ingestion, and whether this accounts for the observed differences in eosinophils and basophils is not known and requires further study.

One limitation of this study is that commercial polystyrene beads were used. MP potentially consumed by humans in the natural environment are often modified by weathering and chemical modification and can also bind chemicals, microorganisms or other substances. In this latter scenario, MP can effectively deliver these co-pollutants to multiple organs and tissues, thereby enhancing their toxicity. Nevertheless, the fact that the “pristine” beads used in our exposure protocol, promoted indices of pre-clinical vascular disease supports our overall hypothesis. A second limitation of this study is that it is difficult to accurately model natural MP exposures. The composition of contaminating MP in the natural environment is complex, given the diversity of polymers, sizes, and mixtures in addition to, as noted above, varied states of degradation, modification and absorption of co-contaminants. The most effective dose and bead size used here (0.5μm beads at a dose of 1.0μg/ml) yields a particle concentration > 10^5 particles /ml, and given 12 wk of consumption, would be at the higher end of estimated human consumption (45). Nevertheless, we observed some adverse effects after shorter times of consumption and with other combinations of size and dose, where effective particle concentrations might more accurately reflect the mean of human consumption. A more accurate dose and size assessment awaits further study. Finally, we have not determined whether those gene expression changes identified in PVAT were replicated in other fat depots as well, and thus if PS consumption promotes the dysfunction of these depots as well.

5. CONCLUSIONS

In summary, we found that the ingestion of PS beads by mice promotes a phenotype characterized by increased adiposity and higher HOMA-IR scores and that this occurs in a dose- and size-dependent manner. The observed increase in adiposity may result from gene expression changes impairing Wnt signaling and/or promoting adipose whitening as well as changes in gut microbiota. Some changes in immune responses were also observed. Thus, the inevitable ingestion of microplastics in the modern world may promote CMD and may thus be considered as a new risk factor for the development of CVD.

Supplementary Material

Refer to Web version on PubMed Central for supplementary material.

ACKNOWLEDGEMENTS

The authors acknowledge the assistance of Gregg Shirk and Israel Sithu Ph.D. Research reported in this publication was supported by the National Institutes of Health under Award Numbers R01ES019217, P30ES030283, P30GM127607 and P20GM103436. The microbiome analysis was carried out in the Functional Microbiomics Core facility supported by the NIH/NIGMS CoBRE grant (P20GM125504-01). Additional support from the Jewish Heritage Fund for Excellence (DJC). The content is solely the responsibility of the authors and does not necessarily represent the official views of the National Institutes of Health.

REFERENCES

1. Rubio L, Marcos R, Hernandez A. Potential adverse health effects of ingested micro- and nanoplastics on humans. Lessons learned from in vivo and in vitro mammalian models. J Toxicol Environ Health B Crit Rev. 2020;23:51–68. [PubMed: 31822207]
2. Duis K, Coors A. Microplastics in the aquatic and terrestrial environment: sources (with a specific focus on personal care products), fate and effects. Environ Sci Eur. 2016;28:2. [PubMed: 27752437]
3. Deng Y, Zhang Y, Lemos B, Ren H. Tissue accumulation of microplastics in mice and biomarker responses suggest widespread health risks of exposure. Sci Rep. 2017;7:46687. [PubMed: 28436478]
4. Jani P, Halbert GW, Langridge J, Florence AT. The uptake and translocation of latex nanospheres and microspheres after oral administration to rats. J Pharm Pharmacol. 1989;41:809–12. [PubMed: 2576440]
5. Prata JC, da Costa JP, Lopes I, Duarte AC, Rocha-Santos T. Environmental exposure to microplastics: An overview on possible human health effects. Sci Total Environ. 2020;702:134455. [PubMed: 31733547]
6. Eyles J, Alpar O, Field WN, Lewis DA, Keswick M. The transfer of polystyrene microspheres from the gastrointestinal tract to the circulation after oral administration in the rat. J Pharm Pharmacol. 1995;47:561–5. [PubMed: 8568621]
7. Fournier SB, D'Errico JN, Adler DS, Kollontzi S, Goedken MJ, Fabris L, et al. Nanopolystyrene translocation and fetal deposition after acute lung exposure during late-stage pregnancy. Part Fibre Toxicol. 2020;17:55. [PubMed: 33099312]
8. Hesler M, Aengenheister L, Ellinger B, Drexel R, Straskraba S, Jost C, et al. Multi-endpoint toxicological assessment of polystyrene nano- and microparticles in different biological models in vitro. Toxicol In Vitro. 2019;61:104610. [PubMed: 31362040]
9. Stock V, Bohmert L, Lisicki E, Block R, Cara-Carmona J, Pack LK, et al. Uptake and effects of orally ingested polystyrene microplastic particles in vitro and in vivo. Arch Toxicol. 2019;93:1817–33. [PubMed: 31139862]
10. Brown DM, Wilson MR, MacNee W, Stone V, Donaldson K. Size-dependent proinflammatory effects of ultrafine polystyrene particles: a role for surface area and oxidative stress in the enhanced activity of ultrafines. Toxicol Appl Pharmacol. 2001;175:191–9. [PubMed: 11559017]
11. Prietl B, Meindl C, Roblegg E, Pieber TR, Lanzer G, Frohlich E. Nano-sized and micro-sized polystyrene particles affect phagocyte function. Cell Biol Toxicol. 2014;30:1–16. [PubMed: 24292270]
12. Lim SL, Ng CT, Zou L, Lu Y, Chen J, Bay BH, et al. Targeted metabolomics reveals differential biological effects of nanoplastics and nanoZnO in human lung cells. Nanotoxicology. 2019;13:1117–32. [PubMed: 31272252]
13. Prata JC. Airborne microplastics: Consequences to human health? Environ Pollut. 2018;234:115–26. [PubMed: 29172041]
14. Jin Y, Lu L, Tu W, Luo T, Fu Z. Impacts of polystyrene microplastic on the gut barrier, microbiota and metabolism of mice. Sci Total Environ. 2019;649:308–17. [PubMed: 30176444]

15. Lu L, Wan Z, Luo T, Fu Z, Jin Y. Polystyrene microplastics induce gut microbiota dysbiosis and hepatic lipid metabolism disorder in mice. Sci Total Environ. 2018;631–632:449-58.
16. Bhatnagar A. Environmental Determinants of Cardiovascular Disease. Circ Res. 2017;121:162–80. [PubMed: 28684622]
17. Merkley SD, Moss HC, Goodfellow SM, Ling CL, Meyer-Hagen JL, Weaver J, et al. Polystyrene microplastics induce an immunometabolic active state in macrophages. Cell Biol Toxicol. 2021. 10.1007/s10565-021-09616-x
18. Pabortsava K, Lampitt RS. High concentrations of plastic hidden beneath the surface of the Atlantic Ocean. Nat Commun. 2020;11:4073. [PubMed: 32811835]
19. Biale G, La Nasa J, Mattonai M, Corti A, Vinciguerra V, Castelvetro V, et al. A Systematic Study on the Degradation Products Generated from Artificially Aged Microplastics. Polymers (Basel). 2021;13(12).
20. Cherry N, Gautrin D. Neurotoxic effects of styrene: further evidence. Br J Ind Med. 1990;47(1):29–37. [PubMed: 2155647]
21. Huff J, Infante PF. Styrene exposure and risk of cancer. Mutagenesis. 2011;26:583–4. [PubMed: 21724974]
22. Ghosh Dastidar S, Jagatheesan G, Haberzettl P, Shah J, Hill BG, Bhatnagar A, et al. Glutathione S-transferase P deficiency induces glucose intolerance via JNK-dependent enhancement of hepatic gluconeogenesis. Am J Physiol Endocrinol Metab. 2018;315:E1005–E18. [PubMed: 30153066]
23. Abplanalp WT, Wickramasinghe NS, Sithu SD, Conklin DJ, Xie Z, Bhatnagar A, et al. Benzene Exposure Induces Insulin Resistance in Mice. Toxicol Sci. 2019;167:426–37. [PubMed: 30346588]
24. Wick RR, Judd LM, Gorrie CL, Holt KE. Completing bacterial genome assemblies with multiplex MinION sequencing. Microb Genom. 2017;3:e000132. [PubMed: 29177090]
25. De Coster W, D'Hert S, Schultz DT, Cruts M, Van Broeckhoven C. NanoPack: visualizing and processing long-read sequencing data. Bioinformatics. 2018;34:2666–9. [PubMed: 29547981]
26. Shanmuganandam S, Hu Y, Strive T, Schwessinger B, Hall RN. Uncovering the microbiome of invasive sympatric European brown hares and European rabbits in Australia. PeerJ. 2020;8:e9564. [PubMed: 32874776]
27. Conklin DJ, Haberzettl P, Prough RA, Bhatnagar A. Glutathione-S-transferase P protects against endothelial dysfunction induced by exposure to tobacco smoke. Am J Physiol Heart Circ Physiol. 2009;296(5):H1586–97. [PubMed: 19270193]
28. Lohn M, Dubrovska G, Lauterbach B, Luft FC, Gollasch M, Sharma AM. Periadventitial fat releases a vascular relaxing factor. FASEB J. 2002;16:1057–63. [PubMed: 12087067]
29. Abplanalp W, Haberzettl P, Bhatnagar A, Conklin DJ, O'Toole TE. Carnosine Supplementation Mitigates the Deleterious Effects of Particulate Matter Exposure in Mice. J Am Heart Assoc. 2019;8:e013041. [PubMed: 31234700]
30. Cui Y, Jia F, He J, Xie X, Li Z, Fu M, et al. Ambient Fine Particulate Matter Suppresses In Vivo Proliferation of Bone Marrow Stem Cells through Reactive Oxygen Species Formation. PLoS One. 2015;10:e0127309. [PubMed: 26058063]
31. Haberzettl P, O'Toole TE, Bhatnagar A, Conklin DJ. Exposure to Fine Particulate Air Pollution Causes Vascular Insulin Resistance by Inducing Pulmonary Oxidative Stress. Environ Health Perspect. 2016;124:1830–9. [PubMed: 27128347]
32. Ahmadieh S, Kim HW, Weintraub NL. Potential role of perivascular adipose tissue in modulating atherosclerosis. Clin Sci (Lond). 2020;134:3–13. [PubMed: 31898749]
33. Davis CD. The Gut Microbiome and Its Role in Obesity. Nutr Today. 2016;51:167–74. [PubMed: 27795585]
34. DiBaise JK, Zhang H, Crowell MD, Krajmalnik-Brown R, Decker GA, Rittmann BE. Gut microbiota and its possible relationship with obesity. Mayo Clin Proc. 2008;83:460–9. [PubMed: 18380992]
35. Khan MJ, Gerasimidis K, Edwards CA, Shaikh MG. Role of Gut Microbiota in the Aetiology of Obesity: Proposed Mechanisms and Review of the Literature. J Obes. 2016;2016:7353642. [PubMed: 27703805]

36. Kaur J. A comprehensive review on metabolic syndrome. Cardiol Res Pract. 2014;2014:943162. [PubMed: 24711954]
37. Chen N, Wang J. Wnt/beta-Catenin Signaling and Obesity. Front Physiol. 2018;9:792. [PubMed: 30065654]
38. Christodoulides C, Lagathu C, Sethi JK, Vidal-Puig A. Adipogenesis and WNT signalling. Trends Endocrinol Metab. 2009;20:16–24. [PubMed: 19008118]
39. Tong Q, Dalgin G, Xu H, Ting CN, Leiden JM, Hotamisligil GS. Function of GATA transcription factors in preadipocyte-adipocyte transition. Science. 2000;290:134–8. [PubMed: 11021798]
40. Nishigori H, Tomura H, Tonooka N, Kanamori M, Yamada S, Sho K, et al. Mutations in the small heterodimer partner gene are associated with mild obesity in Japanese subjects. Proc Natl Acad Sci U S A. 2001;98:575–80. [PubMed: 11136233]
41. Naaz A, Holsberger DR, Iwamoto GA, Nelson A, Kiyokawa H, Cooke PS. Loss of cyclin-dependent kinase inhibitors produces adipocyte hyperplasia and obesity. FASEB J. 2004;18:1925–7. [PubMed: 15469964]
42. Chiappini F, Cunha LL, Harris JC, Hollenberg AN. Lack of cAMP-response element-binding protein 1 in the hypothalamus causes obesity. J Biol Chem. 2011;286:8094–105. [PubMed: 21209091]
43. Seale P Transcriptional Regulatory Circuits Controlling Brown Fat Development and Activation. Diabetes. 2015;64:2369–75. [PubMed: 26050669]
44. Bartelt A, Widenmaier SB, Schlein C, Johann K, Goncalves RLS, Eguchi K, et al. Brown adipose tissue thermogenic adaptation requires Nrf1-mediated proteasomal activity. Nat Med. 2018;24:292–303. [PubMed: 29400713]
45. Cox KD, Covernton GA, Davies HL, Dower JF, Juanes F, Dudas SE. Human Consumption of Microplastics. Environ Sci Technol. 2019;53:7068–74. [PubMed: 31184127]

HIGHLIGHTS

- Consumption of polystyrene beads promotes adiposity and hyperglycemia.
- Consumption of polystyrene beads promotes changes in the gut microbiome.
- Consumption of polystyrene beads promotes changes in PVAT gene expression.
- Microplastics exposure may be a new risk factor for cardiovascular disease

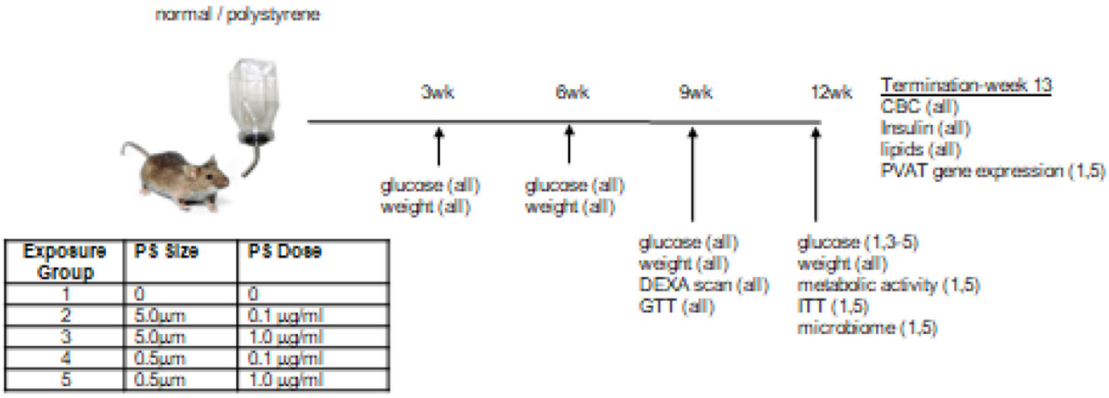

Exposure Group	PS Size	PS Dose
1	0	0
2	5.0μm	0.1 μg/ml
3	5.0μm	1.0 μg/ml
4	0.5μm	0.1 μg/ml
5	0.5μm	1.0 μg/ml

Figure 1. Experimental approach.

Mice were supplied with normal drinking water or that containing polystyrene (PS) beads of a given size and dose (table) for 12 weeks. Illustrated are the times of analytical measures with the groups used for those measures in parentheses.

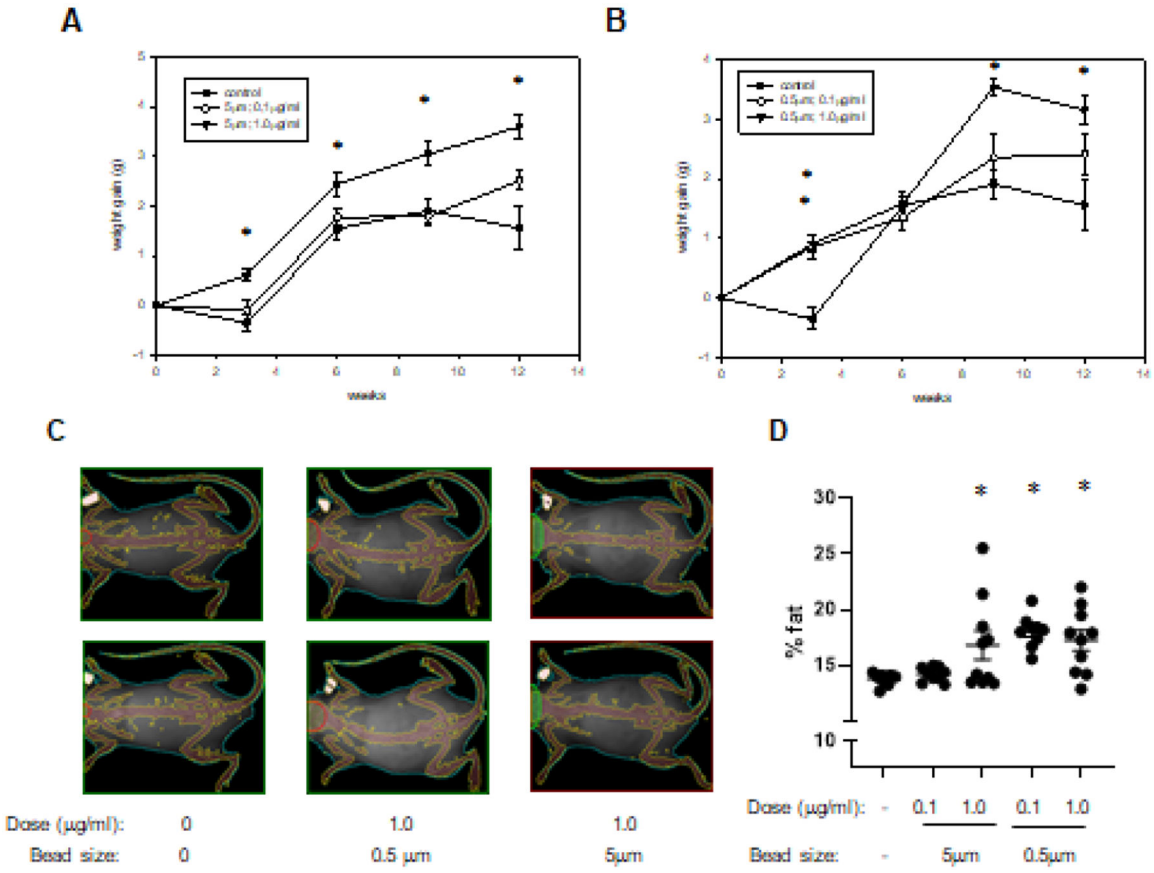

Figure 2. Body weight and composition.

The weights of mice drinking normal water (control) and that containing 5μm PS beads (A) or 0.5μm PS beads (B) at the indicated concentrations were obtained after 3, 6, 9, and 12 weeks of consumption. Depicted are representative DEXA scan images from the indicated groups after 9 weeks of consumption (C). Also illustrated is the percent body fat determined for all mice and all groups (D). *: $p<0.05$.

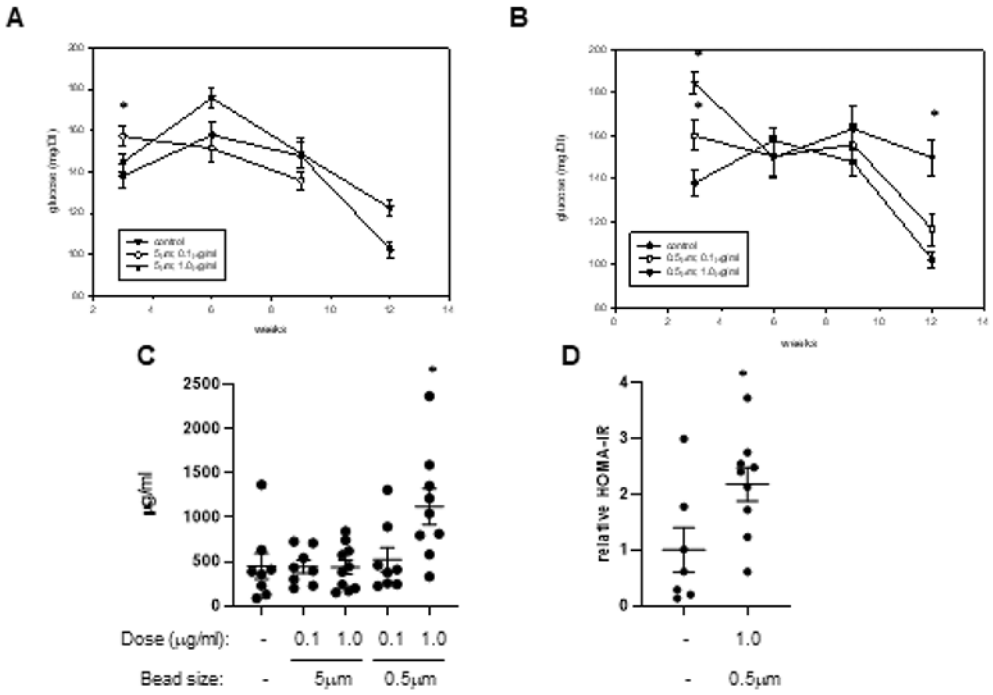

Figure 3. Plasma glucose and insulin.

Fasting plasma glucose levels were obtained from mice drinking normal water (control) and that containing 5μm PS beads (A) or 0.5μm PS beads (B) at the indicted concentration after 3, 6, 9, and 12 weeks of consumption. Fasting plasma insulin levels were measured in samples collected from the 5 treatment groups at termination (C). Also illustrated are calculated HOMA-IR scores obtained from control mice and those mice ingesting 0.5μm beads at a dose of 1μg/ml for 12 weeks (D). *: $p<0.05$

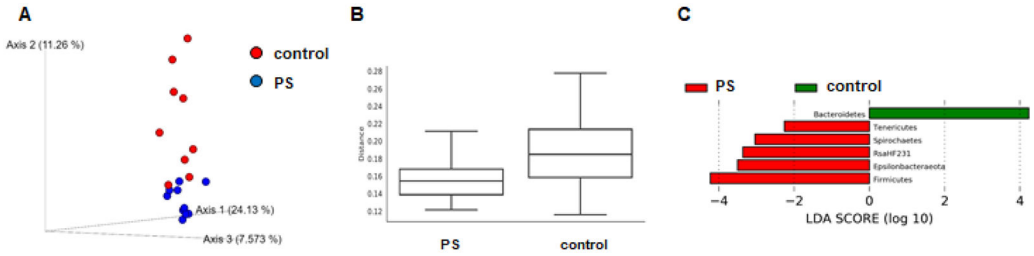

Figure 4. Microbiome analysis.

A) Illustrated is the principal coordinate analysis of beta diversity of gut microbiota from unweighted UniFrac distance values. Samples from mice consuming water containing the PS beads (blue) are more tightly clustered than the control samples which show higher variation. B) Illustrated are boxplots of beta diversity of the gut microbiota from the unweighted UniFrac distance values of two groups with q-value 0.028 as calculated from a PERMANOVA test. C) Linear discriminant analysis (LDA) effect size (LEfSe) analysis identifies differentially abundant gut microbiota with LDA score ≥ 2 in Phylum level between two groups based on a non-parametric Kruskal-Wallis test.

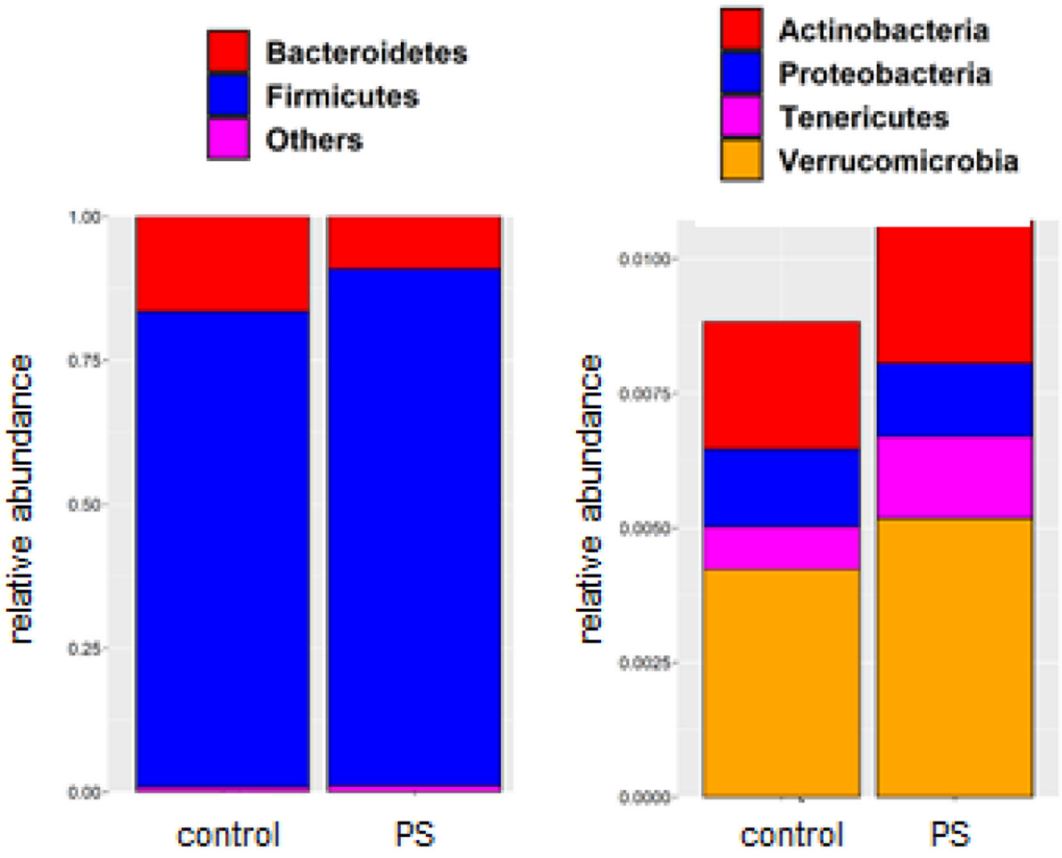

Figure 5. Phylum level composition.

Illustrated is the relative abundance of Bacteriodetes and Firmicutes in the collected fecal samples (left) and the relative abundance of more lowly expressed phyla (right). PS: water containing polystyrene beads.

Table 1.

Complete blood cell count

Exposure		Cell type							
size	**dose**	**WBC**	**NE**	**LY**	**MO**	**EO**	**BA**	**RBC**	**PLT**
-	-	1.89 (0.38)	0.760 (0.271)	1.06 (0.20)	0.049 (0.011)	0.003 (0.002)	0.001 (0.001)	7.07 (0.75)	768 (64.6)
5 μm	0.1μg/ml	2.68 (0.59)	1.49 (0.46)	1.04 (0.14)	0.091 (0.026)	0.034 * (0.011)	0.016 * (0.007)	9.23 (0.37)	583 (87.2)
5 μm	1.0 μg/ml	2.32 (0.27)	0.764 (0.095)	1.39 (0.18)	0.098 * (0.015)	0.047 * (0.011)	0.015 * (0.005)	8.07 (0.49)	536 (73.1)
0.5 μm	0.1 μg/ml	2.23 (0.45)	0.912 (0.304)	1.24 (0.18)	0.074 (0.013)	0.002 (0.001)	0.001 (0.001)	7.64 (0.57)	632 (84.4)
0.5 μm	1.0 μg/ml	1.69 (0.24)	0.506 (0.137)	1.11 (0.13)	0.058 (0.010)	0.006 (0.004)	0 (0)	7.97 (0.48)	843 (61.3)

Listed are cell counts in blood samples obtained from the 5 treatment groups at termination. Values are presented as average (SE). WBC: white blood cells; NE: neutrophils; LY: lymphocytes; MO: monocytes; RBC: red blood cells; PLT: platelets; EO: eosinophils; BA: basophils. Units are 10^3 cells per μl except for RBC which is 10^6 per μl.

*: $p<0.05$ vs control.

Table 2.

Significant PVAT gene expression changes

	Abbreviation	Fold change (array)	Fold change (rtPCR) avg (SE)
Adipogenesis-related genes			
Up-regulated			
Dickkopf1 homolog 1	Dkk1	4.234	
Insulin receptor substrate 2	Irs2	1.825	2.03 (0.69)
Kruppel-like factor 2	Klf2	1.766	
Vitamin D receptor	Vdr	1.656	
Jun oncogene	Jun	1.566	
Down-regulated			
GATA binding protein 3	Gata3	0.051	
Bone morphogenetic protein 7	Bmp7	0.172	0.56 (0.07)
Wingless-related MMTV integration site 1	Wnt1	0.407	0.70 (0.17)
E2F transcription factor 1	E2f1	0.413	
Nuclear receptor subfamily 0, group B, member 2	Nr0b2	0.425	
Rous sarcoma oncogene	Src	0.480	
Cyclin-dependent kinase 1b	Cdkn1b	0.491	
Nuclear respiratory factor 1	Nrf1	0.511	
CAMP responsive element binding protein 1	Creb1	0.554	
Early growth response 2	Egr2	0.560	
Axin 1	Axin1	0.569	
Wingless-related MMTV integration site 5B	Wnt5b	0.596	
TSC22 domain family, member 3	Tsc22d3	0.641	
Runt-related transcription factor 1	Runx1t1	0.647	
Inflammation-related genes			
Interleukin-6	IL-6	ND	1.48 (0.29)
Monocyte chemoattractant protein-1	Mcp-1	ND	1.28 (0.15)

Listed are those genes in the array analysis which were up-regulated (fold change >1.5 fold) or down-regulated (fold change <0.666) using pooled RNA samples. Also listed are fold changes of selected genes as determined by rtPCR using individual RNA samples. ND: not determined.